CONF-900791--2

UCRL-JC-103762
PREPRINT

Multiple-Energy Techniques in Industrial Computerized Tomography

Dan Schneberk
Harry Martz
Steve Azevedo

This paper was prepared for submittal to
Review of Progress in Quantitative NDE
University of California, San Diego
La Jolla, California, July 15–20, 1990

August 1, 1990

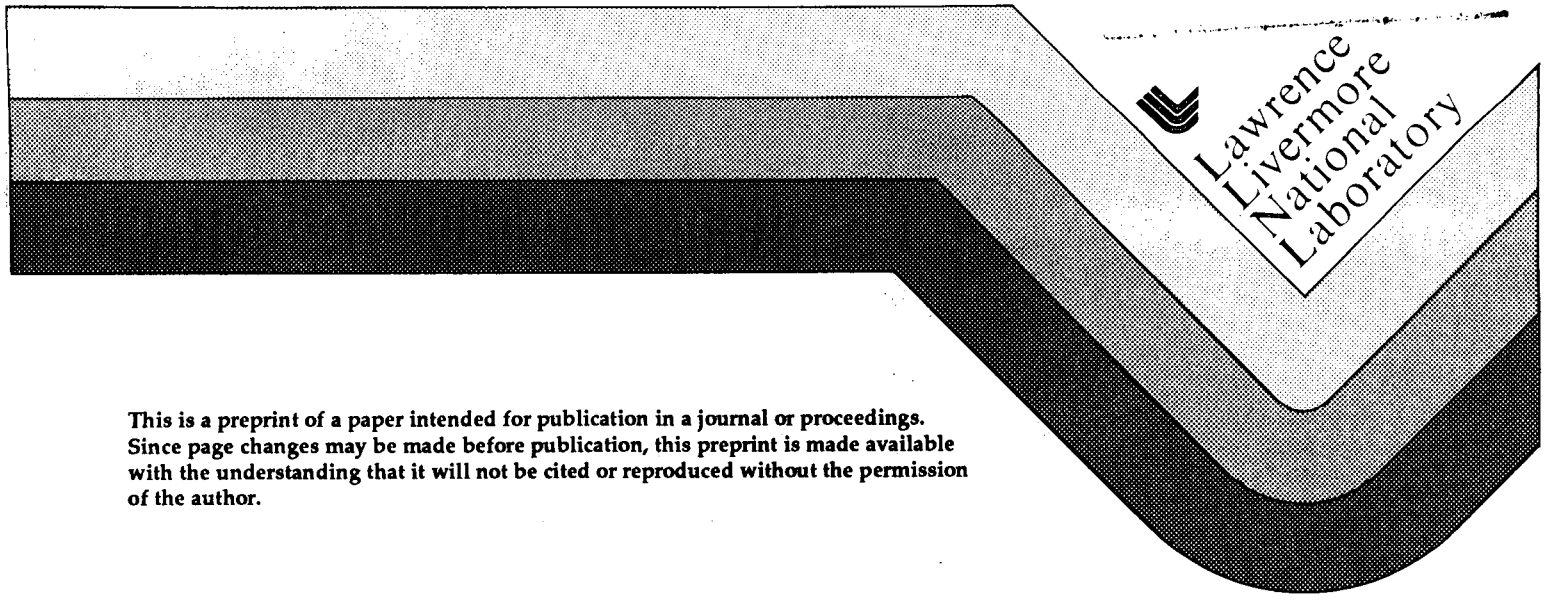

DISCLAIMER

MULTIPLE-ENERGY TECHNIQUES IN INDUSTRIAL COMPUTERIZED TOMOGRAPHY

Dan Schneberk, Harry Martz, and Steve Azevedo
Nondestructive Evaluation Section, L-333
Lawrence Livermore National Laboratory
P.O. Box 808, Livermore, CA 94551

UCRL-JC--103762

DE90 017518

INTRODUCTION

Considerable effort is being applied to develop multiple-energy industrial CT techniques for materials characterization. Multiple-energy CT can provide reliable estimates of effective Z (Z_{eff}), weight fraction, and rigorous calculations of absolute density, all at the spatial resolution of the scanner. Currently, a wide variety of techniques exist for CT scanners [1], but each has certain problems and limitations. Ultimately, the best multi-energy CT technique would combine the qualities of accuracy, reliability, and a wide range of application, and would require the smallest number of additional measurements.

We have developed techniques for calculating material properties of industrial objects that differ somewhat from currently used methods. In this paper, we present our methods for calculating Z_{eff}, weight fraction, and density. We begin with the simplest case – methods for multiple-energy CT using isotopic sources – and proceed to multiple-energy work with x-ray machine sources. The methods discussed here are illustrated on CT scans of (1) PBX-9502 high explosives, (2) a lexan-aluminum phantom, and (3) a cylinder of glass beads used in a preliminary study to determine if CT can resolve three phases: air, water, and a high-Z oil.

In the CT project at LLNL, we have constructed several CT scanners of varying scanning geometries using γ- and x-ray sources, as described elsewhere [2,3]. In our research, we employed two of these scanners: PBCAT (pencil-beam CAT) for CT data using isotopic sources and VCAT (video-CAT) equipped with an IRT™ micro-focal x-ray machine source. Both scanners are described in detail elsewhere[2].

MULTIPLE-ENERGY CT: BACKGROUND AND FUNDAMENTALS

Isotopic Sources

In this section, we assume the use of an isotopic source and an energy-discriminating detector (monochromatic source energies). We begin with the raw transmission measurements. An incident beam of monochromatic x-rays, N_0, will be attenuated by a multilayered, multicomponent object according to the following relationship:

$$N = N_0 \exp\left\{ \sum_{j}^{\text{layers}} \sum_{k}^{\text{elements}} [(\mu/\rho)_{kj}(Z_{kj},E)\,\alpha_{kj}]\,\rho_j\,l_j \right\}, \qquad (1)$$

where N is the number of transmitted photons, $(\mu/\rho)_{kj}$ is the mass absorption coefficient, α_{kj} is the molecular weight fraction (computed

from the chemical formula), and Z_{kj} is the atomic number (the subscripts represent the kth element in the jth compound of the jth layer). ρ_j is the volume density of the jth compound in the jth layer, and l_j is the thickness of the jth layer.

Equation (1) is an application of the "Mixture Rule," described in a variety of different texts (e.g., [4]). A number of total and weighted physical quantities arise from rearranging terms in (1), as follows:

$$\text{Total mass} = M_T = \Sigma \rho_j l_j; \quad \text{Average volume density} = \rho_{avg} = (\Sigma \rho_j l_j)/\Sigma l_j;$$

$$\text{Weight fraction of the jth layer} = w_j = \rho_j l_j / \Sigma \rho_j l_j \ . \tag{2}$$

It is possible to replace the summations over compounds and elements into a single summation over elements [4].

When we employ the above and let T(E) and A(E) denote the transmission and absorptance at energy E, we find the following:

$$N = N_0 \exp\left[-M_T \Sigma (\mu/\rho)_n (Z_n, E)\ w_n\right] \ , \tag{3}$$

$$T(E) = N/N_0 = \exp\left[-M_T \Sigma (\mu/\rho)_n (Z_n, E)\ w_n\right] \ , \tag{4}$$

$$A(E) = -\ln(N/N_0) = M_T \Sigma (\mu/\rho)_n w_n = l_T \rho_{chord} \Sigma (\mu/\rho)_n (Z_n, E)\, w_n \ , \tag{5}$$

where l_T denotes the total path length of the object, $l_T = \Sigma l_j$, and w_n is the weight fraction of the nth element along the chord.

We define Z_{eff} to be the atomic number of the single element that attenuates most like the multicomponent object; that is,

$$(\mu/\rho)(Z_{eff}, E) \cong \Sigma (\mu/\rho)_n (Z_n, E)\ w_n \ . \tag{6}$$

CT scanners based on γ- or x-ray transmission gauging hardware result in linear attenuation coefficient images of the object, which are products of the average density and the linear combination of mass absorption coefficients (representing the chemical composition) per voxel. Using the above notation, we define two linear attenuation coefficients:

$$\mu_{chord}(Z_{eff}, E) = \rho_{chord}\ \Sigma (\mu/\rho)_n (Z_n, E)\ w_n \ , \tag{7a}$$

$$\mu_{obj}(Z_{eff}, E) = \rho_{voxel}\ \Sigma (\mu/\rho)_v (Z_v, E)\ w_v \ , \tag{7b}$$

where v is the index for the elements within a voxel. In multiple-energy CT scanning, such attenuation measurements are taken at a number of different energies for the same path through the object. We use the ratio and difference from two of these scans to calculate Z_{eff}, weight fraction, and absolute density images.

The ratios of absorptances for the projection data, or the ratios of linear attenuation coefficients for the CT reconstructed images, are particularly important for examining Z-dependence. If $A_r(E_1, E_2)$ is the ratio of absorptances for the projection data per chord and $\mu_r(E_1, E_2)$ is the ratio of linear attenuation coefficients per voxel from CT scans,

$$A_r(E_1,E_2) = [l_T \rho_{chord} \Sigma(\mu/\rho)_n(Z_n,E_1)\, w_n] \,/\, [l_T \rho_{chord} \Sigma(\mu/\rho)_n(Z_n,E_2 w_n], \quad (8)$$

$$\mu_r(E_1,E_2) = [\rho_{voxel} \Sigma(\mu/\rho)_v(Z_v,E_1)\, w_v] \,/\, [\rho_{voxel} \Sigma(\mu/\rho)_v(Z_v,E_2)\, w_v]. \quad (9)$$

When we cancel common terms in the numerator and denominator, both Eqs. (8) and (9) reduce to a ratio of mass absorption coefficients per chord or per voxel. For the CT scans,

$$\mu_r(E_1,E_2) \cong \frac{(\mu/\rho)(Z_{eff},\, E_1)}{(\mu/\rho)(Z_{eff},\, E_2)} . \quad (10)$$

Equation (10) expresses a fundamental result for multiple-energy work. The ratio of absorptances from dual-energy x-ray gauging measurements approaches the ratio of mass absorption coefficients, per chord or per voxel, for some particular Z_{eff}. The absorptance ratio is independent of density. If E_1 and E_2 are known, the ratio is a function of only one unknown, Z_{eff}. This is true regardless of the object's chemical matrix.

For our work, component weight fraction is estimated from the differences of reconstructions. A system of equations is constructed, involving different components of the object — one equation for each energy. If the number of energies is sufficient for the number of components of interest, a solution can be found to the linear system. We have found it important to always include the closing constraint $\Sigma S_n = 1$ to enforce nonnegative saturation coefficients on the solution. For a two-component object (e.g., a & b) and CT data at two different energies, E_1 and E_2, the system we use is as follows:

$$\mu_{rc}(E_1) - \mu_{rc}(E_2) = S_a[\mu_a(E_1) - \mu_a(E_2)] + S_b[\mu_b(E_1) - \mu_b(E_2)], \quad 1 = S_a + S_b , \quad (11)$$

and solving for the two components,

$$S_a = \frac{[\mu_{rc}(E_1) - \mu_{rc}(E_2)] - [\mu_b(E_1) - \mu_b(E_2)]}{[\mu_a(E_1) - \mu_a(E_2) - [\mu_b(E_1) - \mu_b(E_2)]}, \quad \text{and } S_b = 1 - S_a , \quad (12)$$

where μ_{rc} is the reconstructed linear attenuation coefficient, $\mu_{a,b}$ are the tabled linear attenuation coefficients, and $S_{a,b}$ are the weight fractions.

Machine Sources

X-ray machine sources yield a bremsstrahlung (polyenergetic) spectrum. Therefore, each x-ray attenuation measurement is the result of an integration over this energy spectrum, denoted here by S(E). In VCAT/Photometrics, the photons are converted into visible light by a scintillator, and we represent this conversion by a weight function, W(E); therefore,

$$I_{p,0} = \int_0^{E_m} W(E)S(E)\, dE, \quad I_p = \int W(E)S(E) \exp[-\mu_{chord}(Z_{eff},E)\, l_T]\, dE, \quad (13)$$

$$T_p = I_p/I_{p,0} = (1/I_{p,0}) \int W(E)S(E) \exp[-\mu_{chord}(Z_{eff},E)\, l_T]\, dE, \quad (14)$$

$$T_p = \int \overline{\exp\,[-\mu_{chord}(Z_{eff},E)\, l_T]\, dE} , \quad (15)$$

$$A_p = -\ln(I_p/I_{p,0}) = -\ln[(1/I_{p,0}) \int W(E)S(E) \exp[-\mu_{chord}(Z_{eff},E)\, l_T]\, dE , \quad (16)$$

$$A_p = \overline{\mu_{chord}(Z_{eff},E)\, l_T} , \quad (17)$$

where I_p and $I_{p,0}$ are polychromatic intensities. T_p and A_p are the polychromatic transmission and absorptance, respectively. The integration takes place for the transmission; thus, the measured value results in an average transmission weighted by both the source spectrum and the weight function. The absorptance is the log of the averaged transmission. Proceeding as before, we find that the ratio of absorptances reduces to a ratio of mass absorption coefficients that is independent of path length and density. The ratio is dependent on only one variable, Z_{eff}. Unlike the case with isotopic sources, we do not know the energy for the mean absorptance. Of course, to the degree that energy filtering is applied, the isotopic methods may be useful.

ESTIMATING EFFECTIVE *Z*

Isotopic Sources

For isotopic sources, E_1 and E_2, are known, and the absorptance ratio depicted in Eq. (10) depends only on Z_{eff}. The estimation of Z_{eff} reduces to finding a function that relates it to the ratio of the absorptances. Such a function can be constructed from tables of mass absorption coefficients. Figure 1 contains plots of this function for taking ratios of mass absorption coefficients [5] into *Z* for 22/25 keV and for 25/88 keV. To estimate *Z* for isotopic sources, we obtain the ratio of cross sections as a function of *Z* from tables [5] and then use this function and some interpolation rule to take the ratio of the CT images into a Z_{eff} image.

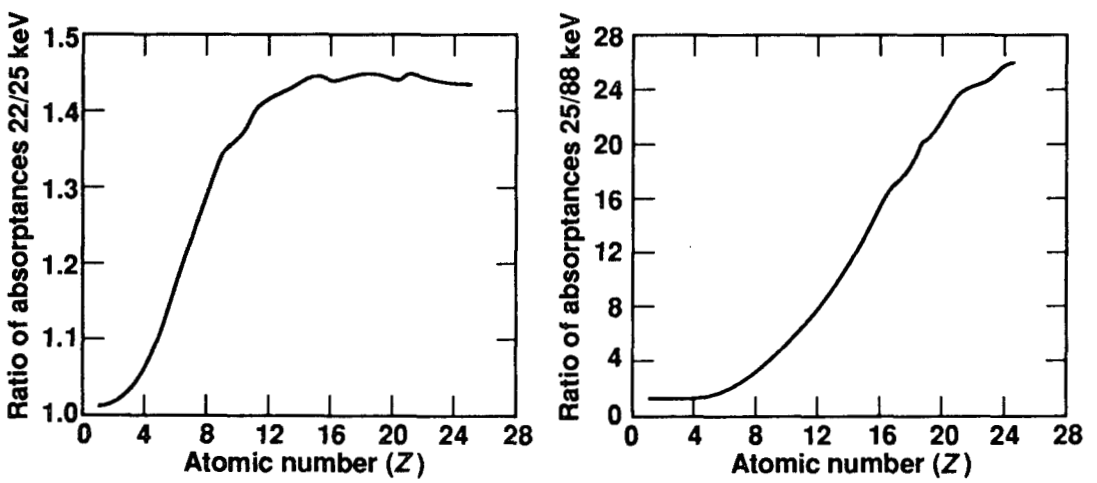

Fig. 1. Plots of the ratio of mass absorption coefficients as a function of *Z*: (a) tabulated values for the 22-to-25-keV ratio, (b) tabulated values for the 25-to-88-keV ratio.

Machine Sources

For machine sources, we assume a model or a measurement of the tube spectrum at the two selected kVp values. In particular, S(E) is assumed known for all values of E in the energy spectrum. Figure 2 contains plots of two energy micro-focal source spectra for both S(E) and S(E)W(E) at 65

and 130 kVp.* Following others [1], we take advantage of the fact that the ratio of absorptances per chord is a function of Z, convert the ray-sums to Z, and reconstruct a Z-per-voxel image with filtered back-projection techniques [6].

From a strictly data-analytic point of view, three variables determine the transmission measurements: (1) Z_{eff}, through the mass absorption coefficients; (2) the average density per chord, ρ_{chord} ; and (3) the path length. A good estimate of the path length can be obtained from the Radon transform of one of the reconstructed images[7]. Consequently, for two transmission measurements at two different kVp values, we have two data sets and two unknowns. Only one pair of Z_{eff} and ρ_{chord} values can generate both transmission measurements. Our procedure is to use the source spectrum and tabulated cross sections [5] to solve for the one (Z_{eff},ρ_{chord}) pair. Unfortunately, beam hardening makes this procedure for machine sources difficult. As mentioned in ref.[1], a beam-hardening correction must be applied to the data prior to reconstructing the final image.

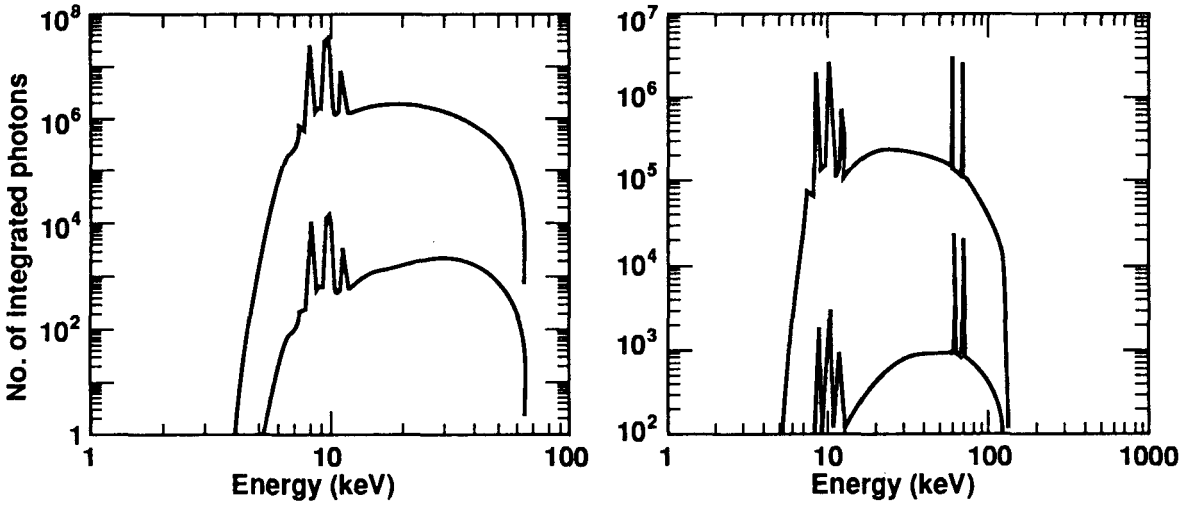

Fig. 2. Plots of the spectra from the TUBDET code (upper curve) and the spectra weighted by the effects of our scintillator (lower curve) for (a) 65 kVp, 1.03 mA and (b) 130 kVp, 0.53 mA.

RESULTS AND DISCUSSION

Isotopic Sources

The first-generation scanners at LLNL[2] provide a particularly good configuration for examining multiple-energy techniques. The data is acquired using γ-ray spectroscopy hardware. Thus, each system is capable of taking several multiple-energy regions of interest simultaneously. Consequently, each CT scan generates several reconstructions of the object, and each image is acquired at the same slice plane but at a different energy. We now examine two different instances of multiple-energy CT: (1) a low-Z, low-contrast case and (2) a low-Z, high-contrast case.

* These spectra were determined using the TUBDET code obtained from NIST.

The first object is a 1/2-in.-diameter cylinder of PBX-9502, a mixture of an explosive (TATB) with a plastic Kel-F binder[8]. We calculated the optimal energy for the longest chord to be between 20 and 26 keV [9]. Using the chemical formula and the weight fractions, we find that the PBX-9502 pellet has a Z_{eff} of 7.6 [8]. A ^{109}Cd source was used to scan the pellet at 22 and 25 keV. The photon statistics obtained, the reconstruction parameters used, and the resultant statistical uncertainty in the data are reported elsewhere[8]. The Z_{eff}, TATB weight fraction, and density images are presented in Fig. 3, with associated grey scales for interpreting the values. The mean calculated Z is 7.8 ± 0.5, close to the expected value. The mean TATB weight fraction is 0.94 ± 0.03, within the target value of 0.95. The mean value of the density image, 1.9 ± 0.2 g/cm^3, matches the bulk wet/dry measured value of 1.904 g/cm^3 [8].

The second object is a lexan-aluminum phantom scanned with the same scanner and ^{109}Cd source. The phantom is a lexan cylinder, 30 mm in diameter, with three aluminum rods (10, 5, and 2 mm in diameter) inserted along the length of the cylinder. The optimal energy for the lexan alone is between 18 and 29 keV for the longest chord. However, for the chord with the 10-mm-diameter rod, the optimal energy is between 60 and 90 keV. Consequently, we performed the multiple-energy work using the results from the 25- and 88-keV reconstructed images. The 25-keV image has streaks as a result of the lack of transmission through the thickest rod, and this pattern will be written into the ratio data. This will be useful to determine how well multiple-energy techniques fare when a wide dynamic range is required and one of the energies is far from optimal.

Figure 4 presents the results, the Z_{eff} image, the histogram of the CT image, and the associated grey scales. The image is dominated by the streaking phenomena; this added variation is reflected in the noisy character of the histogram. In spite of these perturbations, the Zs for lexan (Z = 6) and aluminum (Z = 13) are clearly identified in the histogram. This suggests that, even over a wide dynamic range, multiple-energy techniques can identify the Zs of the components of a high-contrast object. We are investigating the possible applications of multiple-energy techniques using iterative reconstruction methods.

Machine Sources

To assess the viability of CT for examining soils that contain a variety of phases, we prepared a simulated soil sample consisting of oil, water, and air in a matrix of glass beads.* The beads were used to remove heterogeneous matrix uncertainties associated with real soil samples.

We used the VCAT/Photometrics scanner to perform the data acquisition [3]. Scans of the three-phase cylinder were acquired at two energies, 65 and 130 kVp. Figure 2 shows the two source spectra before and after the weighting function for our scintillator was applied. A beam-hardening correction was estimated [10] from the projection data of a cylinder of glass beads and air-scanned using the same data acquisition parameters as the three-phase sample. Separate beam-hardening corrections were estimated for the 65- and 130-kVp data.

* The chemical formulas and densities used in this study are iodododecane doped oil ($C_{20}H_{40}O_2$), 1.0 g/cm^3; H, O_2, and N_2, 0.00122 g/cm^3, for air; and SiO_2, 2.32 g/cm^3, for the glass beads.

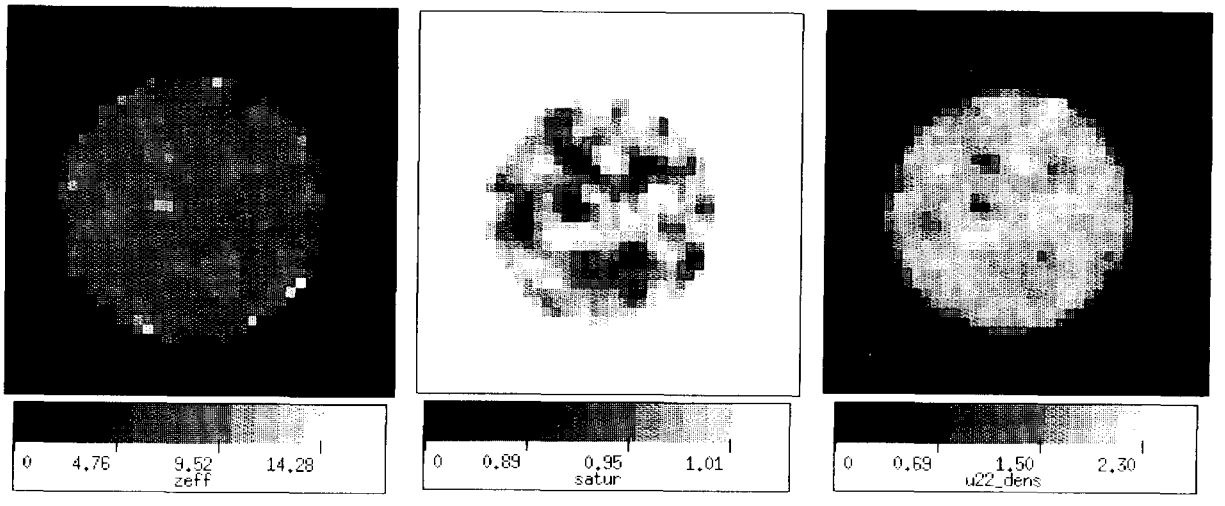

Fig. 3. Resultant Z_{eff} (left), TATB weight fraction (middle), and density (right) images for the medium pellet. The grey scale is given in Z_{eff}, TATB weight fraction, and density (g/cm^3) units, respectively.

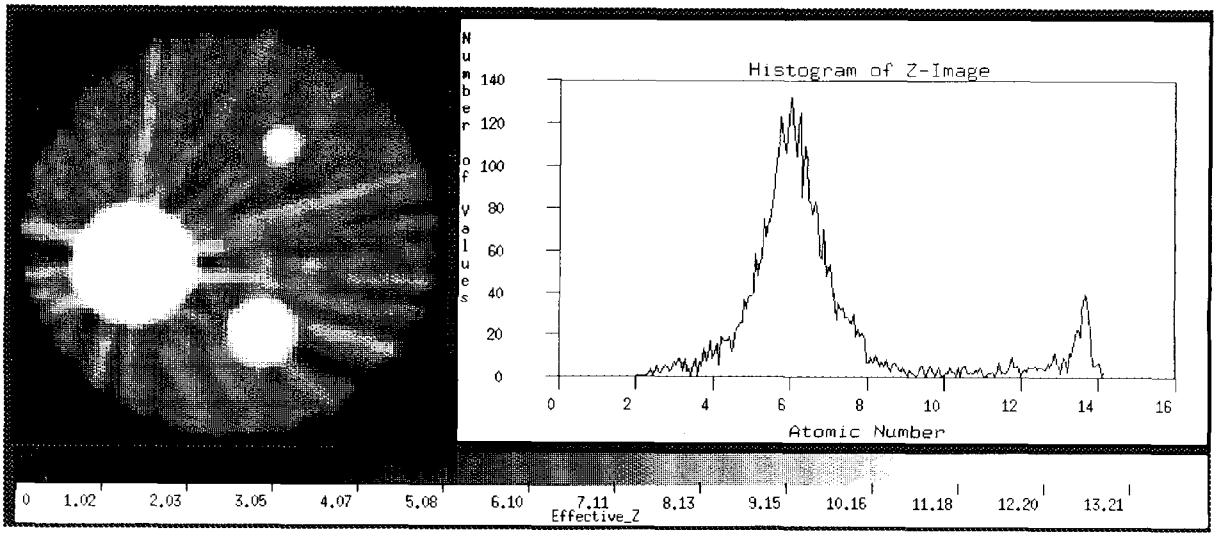

Fig. 4. Z_{eff} image for the lexan-aluminum phantom obtained from the 25- and 88-keV data, with constituent histogram and quantitative grey scale. All values are in units of atomic number.

Figure 5 contains the difference image obtained from 65- and 130-kVp scans and the Z_{eff} image calculated from the per-chord-Z-values projection data. It is interesting to compare the Z_{eff} image with the difference image, which is a stronger function of density. The images suggest variations in both density and Z within the sample. The highest values in the Z_{eff} image represent oil (Z = 23), and the lowest represent water (Z = 7.8) and plastic (Z = 8), with the glass-bead matrix in the middle (Z = 12). Combining this and an analysis of these images reveals that the water and air congregate in the middle, with the oil around the outside, and the glass beads as the background material. These preliminary results show that this technique can discriminate and map all three phases in the sample.

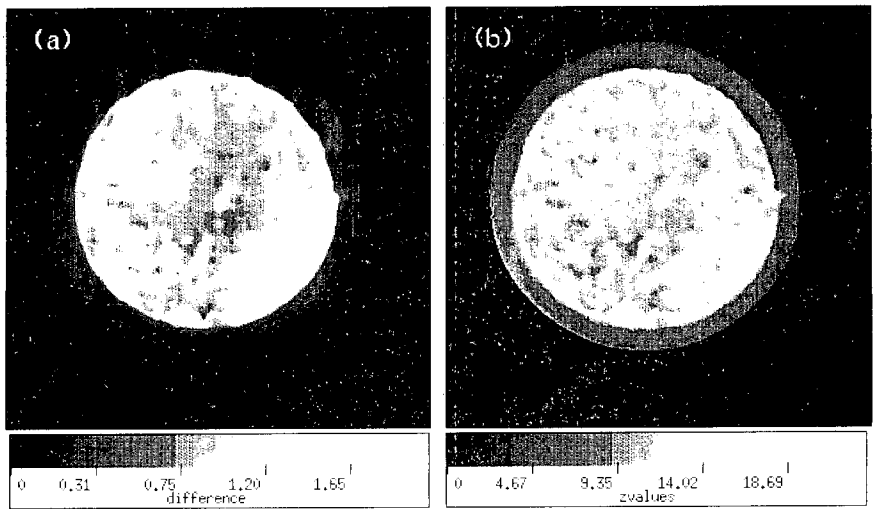

Fig. 5. Resultant difference image from 65- and 130-kVp scans (a) and the Z_{eff} image calculated from the transmission-Z projection data (b).

CONCLUSIONS

We have presented methods for calculating material properties from multiple-energy CT scans using both isotopic and x-ray machine sources. In both cases, tables of mass-absorption coefficients were employed to convert ratios of attenuation measurements into measures of Z_{eff}. In the case of machine sources, we assumed that the source energy spectrum was known, either from a model or from a measurement.

The methods presented here, when applied to the isotopic source data, produce reasonable estimates of Z_{eff}, weight fraction, and density. The estimates of Z_{eff} were verified by the lexan-aluminum phantom, in spite of its wide dynamic range. For the PBX-9502 sample, both the weight fractions and the density matched the measured bulk values. Further, the pixel-to-pixel variation in density showed a distinctly higher variance. Any procedure that calculates density without removing the variation due to changing chemical formula is problematic.

Technical Information Department · Lawrence Livermore National Laboratory
University of California · Livermore, California 94551